Available online at www.sciencedirect.com
ScienceDirect
Journal of Power Sources 174 (2007) 30–40
JOURNAL OF POWER SOURCES
www.elsevier.com/locate/jpowsour

# A novel combined battery model for state-of-charge estimation in lead-acid batteries based on extended Kalman filter for hybrid electric vehicle applications

Amir Vasebi *, Maral Partovibakhsh, S. Mohammad Taghi Bathaee

*Hybrid Electric Vehicle Research Center, Department of Electrical and Electronic Engineering, K.N. Toosi University of Technology, No. 322, Mirdamad Avenue West, 19697 Tehran, Iran*

Received 13 February 2007; received in revised form 30 March 2007; accepted 4 April 2007
Available online 12 April 2007

**Abstract**

In this paper a novel combined battery model for state-of-charge (SoC) estimation in lead-acid batteries, based on extended Kalman filter (EKF) is presented. To obtain a more accurate SoC estimation technique, a combination of the two previously used models (RC and hysteresis battery models) is introduced; trying to compensate deficiencies of the individual models. The changes in the behavior of the battery are considered in the proposed SoC estimation method which makes it suitable for hybrid electric vehicle (HEV) applications. The effectiveness of the proposed method is verified using an experimental test. This Kalman filter modeling approach is shown to give SoC estimation error within 2% compared with Ah counting method; therefore, better results are obtained in comparison with the other conventional methods.


*Keywords:* Batteries; Combined battery model; Extended Kalman filter; Hybrid electric vehicle; State-of-charge

## 1. Introduction

Continuous growing fuel cost and increasing restrictive automobile standards are forcing automobile manufacturers to design new vehicles such as Stop&Start, hybrid, or electric vehicles. The underlying idea is to reduce fuel consumption and exhaust emissions in the urban areas either by stopping the motor when the vehicle is not moving, or by replacement of fossil fuels by rechargeable electric batteries. In order to achieve this goal, car builders have to solve electrical energy storage and management problems. Proposed solutions involve electric energy storage, novel battery designs, fuel cells or super capacitors. Just as it is important to know the amount of fuel remaining in an automobile, the SoC of the battery is an essential factor in HEV and EV operation.

Accurate estimation of the SoC can improve energy management and efficient utilization of batteries in HEV by optimizing the performance, extending the lifetime and preventing permanent damage to the batteries.

During discharge/charge, the energy capability of a battery depends on a number of parameters including discharge/charge current, Coulombic efficiency losses, temperature, battery age, cut-off voltage, and service history (previous charge and discharge) [1,2]. The SoC of the battery is a complex non-linear function of these parameters. Therefore, a variety of techniques has been proposed to measure or monitor the SoC of a cell or battery [2–20], each has its relative merits, as reviewed by Piller et al. [21]. Charge counting or current integration is, at present, the most commonly used technique, requiring dynamic measurement of the cell/battery current which its time integral provides a direct indication of SoC [3–5]. However, because of the reliance on integration, errors in terminal measurements due to noise, resolution and rounding are cumulative and large SoC errors can be resulted. Therefore, a reset or recalibration action is required at regular intervals for all electric vehicles (EVs). This may be carried out during a full charge or conditioning discharge, but it is less appropriate for standard HEV operation where full SoC is rarely achieved [2,7].

The specific gravity of the electrolyte is known to be an accurate measure of SoC in flooded lead-acid cells, but this method is not suitable for valve regulated lead-acid (VRLA) cells, as

* Corresponding author. Tel.: +98 2188462459; fax: +98 2188462066.
*E-mail address:* amir_vasebi@yahoo.com (A. Vasebi).

0378-7753/$ – see front matter © 2007 Elsevier B.V. All rights reserved.
doi:10.1016/j.jpowsour.2007.04.011

the nominal amount of electrolyte is often immobilized in the separator and access to the cell inside is limited. Nevertheless, since the open-circuit terminal voltage of a VRLA battery varies almost linearly over the majority of the battery's SoC [2,9], it has been used in many SoC estimators.

Another broad category of cell modeling and SoC estimation involves measuring cell impedances over a wide range of ac frequencies at different states of charge [10–12,22]. Values of the model parameters are found by least-squares fitting to measured impedance values. SoC may be indirectly obtained from measuring present cell impedance and correlating them with known impedances at various SoC levels. We do not consider this method in our application, as we have no direct method to inject signals into cells to measure impedances.

Other reported methods for estimating SoC have been based on artificial neural networks (ANNs) [13,14] and fuzzy logic principles [15,16]. The main advantage of the ANN-based methods, which makes them distinguishable from the other methods, is that they are capable of estimating SoC when the initial SoC is unknown. However, the implementation of these methods is relatively expensive and needs the training data of a similar battery [23], which may limit the application of these methods. In contrast, in fuzzy-based techniques, easy implementation is a great feature.

Fuzzy logic and ANN-based methods are used to avoid the need for a large number of empirically derived parameters required by the other methods; these methods are best suited for portable equipment applications where precise predicting of SoC is not needed [17]. A good survey of the advantage and limitation of these methods can be found in Ref. [23]. Also, a neural network model for predicting battery power capacity during driving cycles has been added to the Advisor EV and HEV modeling environments [24]. Recently, KF and EKF-based methods have been used to estimate SoC [2,6–8,18]. Kalman filter is an intelligent, and sometimes optimal, means for estimating the state of a dynamic system; therefore many researches have used this predictive nature of KF [25,26] to estimate SoC.

In this paper, first we introduce a new battery model (a combination of RC and hysteresis models), and then we use a method based on EKF for estimating SoC in lead-acid batteries. However, the proposed state-of-charge estimation method and battery model can be easily extended to other types of battery. To test the capability of the proposed model in HEVs, an experimental test is applied to Toyota Prius, where Ni-MH batteries are replaced with 25 Ah lead-acid batteries, in NYCC driving cycle [24]. The paper is organized as follows. In Section 2 the dynamic model of the battery is presented. Implementation of the proposed SoC estimation technique is described in Section 3, and Section 4 presents some experimental tests that confirm the effectiveness of the estimation method. Finally the conclusions are presented in Section 5.

## 2. Battery model

In this section first, a brief overview of the RC and the hysteresis battery model are presented and their advantages and drawbacks are considered separately, finally the new proposed hybrid battery model which is a combination of both RC and hysteresis model are presented.

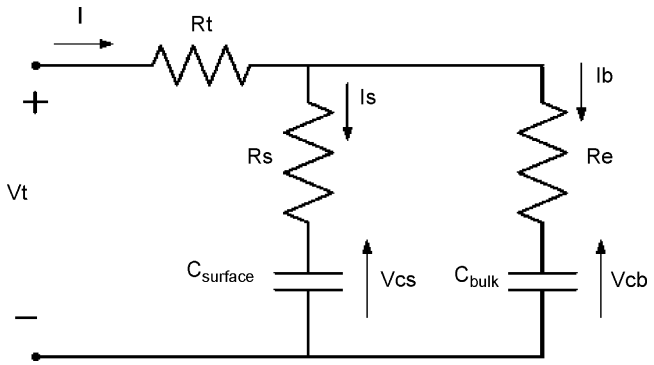


Fig. 1. RC battery model.

### 2.1. RC battery model

RC model is a dynamic model of the battery which consists of a bulk capacitor, $C_{\text{bulk}}$, to characterize the ability of the battery to store charge, a capacitor to model surface capacitance and diffusion effects within the battery, $C_{\text{surface}}$, a terminal resistance, $R_{\text{t}}$, surface resistance, $R_{\text{s}}$, and end resistance, $R_{\text{e}}$ [2] as shown in Fig. 1.

In the case of valve regulated lead-acid (VRLA) batteries, widely used in HEV applications, since the open-circuit terminal voltage of a VRLA battery varies almost linearly over the majority of the battery's SoC (Fig. 2) [2,20], we can employ this characteristic to estimate SoC in VRLA batteries.

#### 2.1.1. Calculation of initial parameters

Initial parameters required for the battery RC model are determined from experimental data. In this paper we have used a 6 V 1 Ah sealed lead-acid battery manufactured by Optima-Palma Battery Co.; where open-circuit voltage (OCV) tests are performed upon successive discharge of battery by injection of current pulses [2,24].

*2.1.1.1. Capacitor $C_{bulk}$.* The capacitance is determined by analyzing the amount of stored energy. Fig. 3 shows the OCV when discharge current pulses of 0.2 A are applied for 3300 s at 6600-s intervals. The energy stored in $C_{\text{bulk}}$ is determined from the OCV at 0% SoC and 100% SoC, using the following expression:

$$E_{C_{\text{bulk}}} = \tfrac{1}{2}C_{\text{bulk}}V^2 = \tfrac{1}{2}C_{\text{bulk}}(V^2_{100\%\,\text{SOC}} - V^2_{0\%\,\text{SOC}}) \quad (1)$$

$E_{C_{\text{bulk}}}$ is equivalent to the rated Amp-sec capacity of the battery, giving

$$C_{\text{bulk-initial}} = \frac{\text{rated(Amp-sec)}V_{100\%\,\text{SOC}}}{(1/2)(V^2_{100\%\,\text{SOC}} - V^2_{0\%\,\text{SOC}})} \quad (2)$$

$V_{100\%\,\text{SOC}}$ and $V_{0\%\,\text{SOC}}$ are illustrated in Fig. 3(b).

*2.1.1.2. Capacitor $C_{surface}$.* The initial value of $C_{\text{surface}}$ relies on the results of high-frequency excitation of the battery to determine the time constant given by the surface capacitor and its

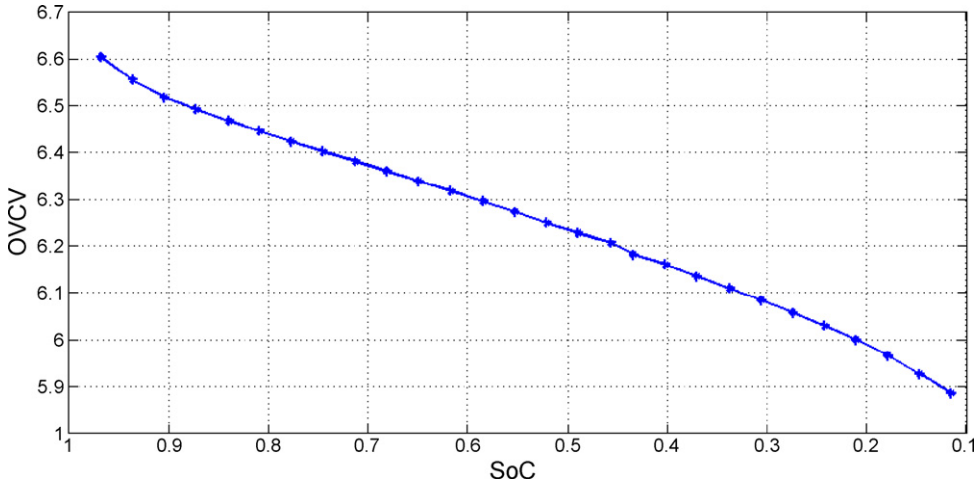


Fig. 2. Open-circuit voltage vs. SoC.

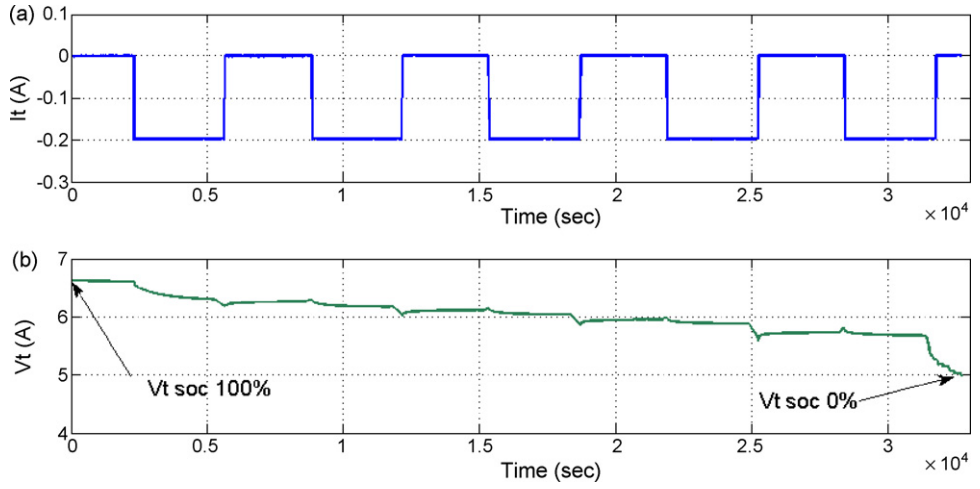


Fig. 3. (a) Discharge current and (b) battery terminal voltage.

associated resistance [2,24]. As before, OCV tests are performed and discharge pulses of 1.1 A are applied at 500-ms intervals, thereby isolating the results from the effects of $C_{\text{bulk}}$. From Fig. 4, it is seen that

$$V_1 = 6.55, \quad V_2 = 6.34, \quad V_3 = 6.49,$$
$$V_4 = 6.52 \quad (\Delta t = 0.5\,\text{s})$$

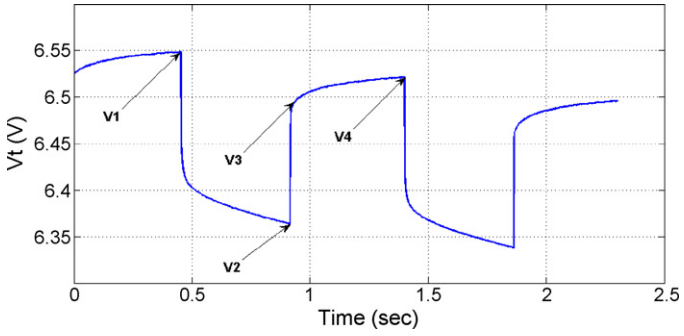


Fig. 4. Battery terminal voltage when a pulse discharge current of 1.1 A is applied.

The time constant is approximated using the following relationship:

$$V_{\text{no-load}} = V_1 = V_3 + (V_4 - V_3)(1 - \text{e}^{t/\tau}) \tag{3}$$

and solving for $\tau$ gives

$$\tau = -\Delta t \ln\left(1 - \frac{V_4 - V_3}{V_1 - V_3}\right) = 0.3466\,\text{s} \tag{4}$$

The time constant is described by

$$\tau = (R_\text{s} + R_\text{e})C_{\text{surface}} \tag{5}$$

Hence, the initial estimate of surface capacitor, is determined as

$$C_{\text{surface-initial}} = \frac{\tau}{R_\text{e} + R_\text{s}} \tag{6}$$

*2.1.1.3. Battery resistance.* The internal resistance of the battery is measured as 0.25 Ω. It is assumed that $R_\text{s}$ and $R_\text{e}$ are

Table 1
Initial parameters for battery model

| Parameters | Value |
|---|---|
| $C_{bulk}$ | 2100 F |
| $C_{surface}$ | 0.5 F |
| $R_e$ | 0.375 Ω |
| $R_s$ | 0.375 Ω |
| $R_t$ | 0.0625 Ω |

equivalent and account for 80% of total resistance. Hence, $R_t$ is

$$0.25 = R_t + \left[\frac{1}{R_e} + \frac{1}{R_s}\right]^{-1} \quad (7)$$

A summary of the initial values is given in Table 1.

*2.1.2. Differential and state-space equations of the model*

Equations that describe the characteristics of the model shown in Fig. 1 are given in [2] (*note*: by convention, the current flowing into the battery is considered to be positive):

$$\dot{V}_{cb} = -\frac{V_{cb}}{2R_eC_{bulk}} + \frac{V_{cs}}{2R_EC_{bulk}} + \frac{I}{2C_{bulk}} \quad (8)$$

$$\dot{V}_{cs} = -\frac{V_{cs}}{2C_{surface}R_e} + \frac{V_{cb}}{2C_{surface}R_e} + \frac{I}{2C_{surface}} \quad (9)$$

$$\dot{V}_t = \left[-\frac{1}{2R_eC_{bulk}} + \frac{1}{2C_{surface}R_e}\right] V_{cb} + \left[\frac{1}{2R_eC_{bulk}} - \frac{1}{2C_{surface}R_e}\right] V_t + \left[\frac{1}{2C_{surface}} - \frac{R_t}{2R_eC_{bulk}} + \frac{R_t}{2R_eC_{surface}}\right] I \quad (10)$$

In these equations, for simplicity we assume that $R_s = R_e$ and the charging rate of terminal current ($dI/dt \approx 0$), per sampling interval when implemented digitally, is negligible.

Here, we have added an extra state $\alpha = 1/C_{bulk}$ into the model state space and assuming that the rate of change of $C_{bulk}$, over a sampling interval, is negligible, e.g. $d\alpha/dt = 0$. Therefore, we have new state-space description of the network as

$$\dot{x} = f(x,u), \quad y = C(x), \quad x = [\,V_{cb} \quad V_{cs} \quad V_t \quad \alpha\,]^T \quad (11)$$

where $x$ is the state vector

$$C(x) = V_t, \quad u = I, \quad f(x,u) = [\,f_1 \quad f_2 \quad f_3 \quad f_3\,]^T \quad (12)$$

that $V_t$ and $u$ are the system output and input, respectively:

$$f_1 = -\frac{x_4x_1}{2R_e} + \frac{x_4x_2}{2R_E} + \frac{x_4I}{2},$$

$$f_2 = -\frac{x_2}{2C_{surface}R_e} + \frac{x_1}{2C_{surface}R_e} + \frac{I}{2C_{surface}},$$

$$f_3 = \left[-\frac{x_4}{2R_e} + \frac{1}{2C_{surface}R_e}\right] x_1 + \left[\frac{x_4}{2R_e} - \frac{1}{2C_{surface}R_e}\right] x_3 + \left[\frac{1}{2C_{Surface}} - \frac{R_tx_4}{2R_e} + \frac{R_t}{2R_eC_{surface}}\right] I, \quad f_4 = 0 \quad (13)$$

*2.1.3. Observability of the RC battery model*

Observability of the system must be investigated after system linearization. Calculating the observability matrix shows that, this matrix is always of full rank, under mild conditions [2].

The main advantage of this model is that it models the dynamic behavior of the battery. It can also detect the battery capacity fade due to cycling. The main drawbacks of the model are that the hysteresis effect is not included, parameter identification is only occurred once and static OCV curve is used to determine SoC.

*2.2. Hysteresis battery model*

The hysteresis effect has serious consequences in predicting SoC and may be seen during rest periods. Following a discharge, the battery voltage always relaxes to a value less than the true OCV for that SoC, and following a charge, the battery voltage always relaxes to a value greater than the true OCV [27].

We illustrate the hysteresis effect by showing the charge/discharge curves at the $C/2$ rate and room temperature in Fig. 5(a), also the hysteresis voltage is plotted versus SoC in Fig. 5(b). As the battery is charged or discharged, the level of hysteresis changes slowly. This slow transition can be modeled by adding a hysteresis state ($h$) to the model state equation. The discrete state equations of the model are as follows [7]:

$$\begin{bmatrix} h_{k+1} \\ SoC_{k+1} \end{bmatrix} = \begin{bmatrix} F(i_k) & 0 \\ 0 & 1 \end{bmatrix} \begin{bmatrix} h_k \\ SoC_k \end{bmatrix} + \begin{bmatrix} 0 & (1-F(i_k)) \\ -\dfrac{\eta_i\,\Delta t}{C_n} & 0 \end{bmatrix} \begin{bmatrix} i_k \\ M(SoC, \dot{SoC}) \end{bmatrix} \quad (14)$$

$$V_{tk} = OCV(SoC_k) - Ri_k + h_k \quad (15)$$

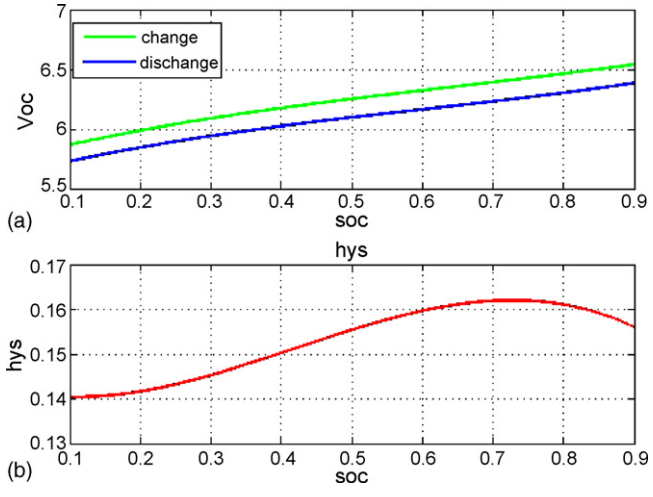


Fig. 5. (a) Hysteresis discharge/charge curves and (b) the hysteresis level.

where $SoC_k$ and $h_k$ are the battery SoC and hysteresis voltage level at step $k$, respectively. $C_n$ is the battery nominal capacity, $\eta_i$ is the battery Coulombic efficiency ($\eta_i = 1$ for discharge, and $\eta_i = \eta \leq 1$ for charge), $\Delta t$ is suitably small sampling period time and $V_t$, $i$ are battery terminal voltage and current (assumed positive for discharge, negative for charge), respectively. $R$ is the battery internal resistance and $M(SoC, \dot{SoC})$ is a function that gives the maximum polarization due to hysteresis as a function of SoC and the rate-of-change of SoC. Specifically, $M(SoC, \dot{SoC})$ is positive for charge ($\dot{SoC} > 0$) and is negative for discharge ($\dot{SoC} < 0$). We define $F(i_k) = \exp(-|\eta_i i_k \gamma \Delta t / C_n|)$, where $\gamma$ is a positive constant. This model is not linear in the parameters therefore advanced nonlinear methods, such as EKF, are used to identify the unknown parameters [7]. The identification method will be explained in Section 3.2.

In spite of having some advantages [7], this model has major disadvantages including the use of static SoC–OCV curves, inability in modeling the capacity fade and difficulties in implementation of the identification method.

### 2.3. The proposed battery model

This new battery model shown in Fig. 6 is a combination of two previously mentioned models. The RC model acts as the primary model. It prepares the required data for parameter identification of the secondary model (hysteresis model) and also models the battery capacity fade by means of the state variable $\alpha$. Using the output data of RC model, the hysteresis model (secondary model) identifies its own unknown parameters and updates them every 10 sample (every 1 s). At the same time, it estimates the battery SoC. Therefore, we have a model which directly includes several effecting factors in the battery modeling such as hysteresis effect, battery capacity degradation and changes in the internal resistance of the battery. Furthermore, as the identification of the model parameters occur sequentially, the

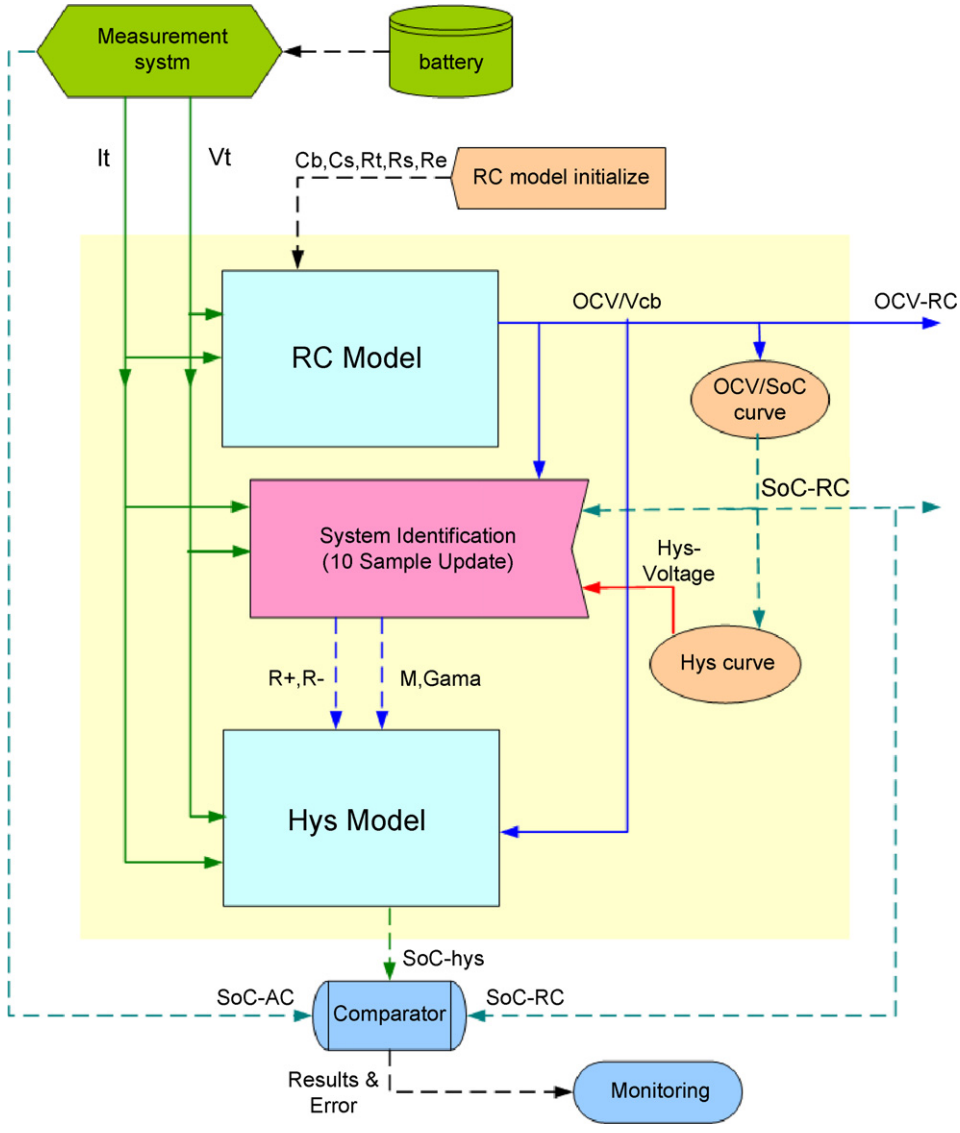


Fig. 6. Block diagram of the SoC estimation method.

effect of the other factors such as temperature, pressure, cycling, etc., is taken into account automatically.

## 3. Implementation

In this section we describe the implementation of the model via EKF. The model implementation procedure can be divided into three main steps as shown in Fig. 6:

(1) OCV and SoC estimation using EKF in the RC model.
(2) Parameter identification of the hysteresis model using the first step outputs.
(3) SoC estimation of the hysteresis model by EKF.

### 3.1. Step1: OCV and SoC estimation using EKF in RC model

In order to apply the EKF, a small-signal model of the system is required. As the model state equations are nonlinear (Eqs. (12) and (13), we use the well-known Jacobian matrixes to linearize these equations about the current operating point $x_0$ and $u_0$:

$$\delta\dot{x} = A_k\delta x + B_k\delta u, \qquad \delta y = C_k\delta x \tag{16}$$

where

$$A_k = \left.\frac{\mathrm{d}f(x,u)}{\mathrm{d}x}\right|_{x_k,u_k}, \quad B_k = \left.\frac{\mathrm{d}f(x,u)}{\mathrm{d}u}\right|_{x_k,u_k},$$
$$C_k = \left.\frac{\mathrm{d}C(x)}{\mathrm{d}x}\right|_{x_k,u_k} = C \tag{17}$$

Now, we calculate these matrixes for our system:

$$A_k = \begin{bmatrix} a_{11} & a_{12} & 0 & a_{14} \\ a_{21} & a_{22} & 0 & 0 \\ a_{31} & 0 & a_{33} & a_{34} \\ 0 & 0 & 0 & 0 \end{bmatrix},$$
$$a_{11} = -a_{12} = -\frac{x_{4k}}{2R_\mathrm{e}}, \quad a_{14} = -\frac{x_{1k} + x_{2k} + I_k R_\mathrm{e}}{2R_\mathrm{e}},$$
$$a_{21} = -a_{22} = \frac{1}{2R_\mathrm{e}C_\mathrm{surface}}, \quad a_{31} = -\frac{x_{4k}}{2R_\mathrm{e}} + \frac{1}{2R_\mathrm{e}C_\mathrm{surface}},$$
$$a_{33} = \frac{x_{4k}}{2R_\mathrm{e}} - \frac{1}{2R_\mathrm{e}C_\mathrm{surface}}, \quad a_{34} = -\frac{x_{1k}}{2R_\mathrm{e}} + \frac{x_{3k}}{2R_\mathrm{e}} - \frac{I_k R_\mathrm{t}}{2R_\mathrm{e}} \tag{18}$$

and

$$B_k = \left[\frac{x_{4k}}{2} \quad \frac{1}{2C_\mathrm{surface}} \quad b_{13} \quad 0\right]^\mathrm{T},$$
$$b_{13} = \frac{1}{2C_\mathrm{Surface}} - \frac{R_\mathrm{t}x_{4k}}{2R_\mathrm{e}} + \frac{R_\mathrm{t}}{2R_\mathrm{e}C_\mathrm{surface}} \tag{19}$$

ultimately,

$$C = [0 \quad 0 \quad 1 \quad 0] \tag{20}$$

Assuming the applied input $u$ is constant during each sampling interval; discrete-time equivalent model of the system is given by

$$x_{k+1} = A_\mathrm{d}x_k + B_\mathrm{d}u_k, \qquad y_{k+1} = Hx_{k+1} \tag{21}$$

where

$$A_\mathrm{dk} \approx I + A_k\,\Delta T, \quad B_\mathrm{dk} = B_k\,\Delta T, \quad H = C \tag{22}$$

and $\Delta T$ is the sampling period. The system is now assumed to be corrupted by stationary Gaussian white noise, via the additive vectors, $\sigma_k$ and $\mu_k$, the former being used to represent system disturbances and model inaccuracies and the latter represents the effects of the measurement noise. Both $\sigma_k$ and $\mu_k$ are considered to have a zero mean value, for all $k$, with the following covariance matrices ($E$ denoting the expectation operator):

$$E[\,\sigma_k \quad \sigma_k^\mathrm{T}\,] = Q \text{ for all } k, \qquad E[\,\mu_k \quad \mu_k^\mathrm{T}\,] = R \text{ for all } k \tag{23}$$

The resulting system is, therefore, described as follows:

$$x_{k+1} = A_\mathrm{dk}x_k + B_\mathrm{dk}u_k + \sigma_k, \qquad z_{k+1} = Hx_{k+1} + \mu_{k+1} \tag{24}$$

where $z$ is the vector of measured outputs after being corrupted by noise.

For notational purpose, we define $\hat{x}_k^-$ (note the "super minus") to be a priori state estimate at step $k$ given knowledge of the process prior to step $k$, and $\hat{x}_k$ to be a posteriori state estimate at step $k$ given by the measurement $z_k$ [25,26]. Now we can define a priori and a posteriori estimate errors as

$$e_k^- = x_k - \hat{x}_k^-, \qquad e_k = x_k - \hat{x}_k \tag{25}$$

The a priori and the a posteriori estimate error covariance are then are then

$$P_k^- = E[\,e_k^- \quad e_k^{-\mathrm{T}}\,], \qquad P_k = E[\,e_k^- \quad e_k^\mathrm{T}\,] \tag{26}$$

A property of the EKF is that it estimates the state vector of the system, $\hat{x}_k$, by minimizing the sum-of-squared errors, $P_k$, between the actual and the estimated states:

$$\min\{P_k\} = \min\{E[\,(x_k - \hat{x}_k) \quad (x_k - \hat{x}_k)^\mathrm{T}\,]\} \tag{27}$$

The recursive EKF algorithm [25,26] is implemented with the predictor/corrector stages as shown in Fig. 7. The EKF estimate, $\hat{x}_{k+1}$, is calculated from the previous state estimate, $\hat{x}_k$, the input vector, $u$, and the measurement signals, $z$. The available input/output data at each sample step is considered to be $u_0$, $u_1$, $u_2$, …, $u_k$, $u_{k+1}$, and $z_0$, $z_1$, $z_2$, …, $z_k$, $z_{k+1}$.

Since only terminal quantities of the battery can be measured, the input is defined as $u = I$ and the measured output is $y = V_\mathrm{t}$. Although no formal stability and tuning methods are available for initializing the EKF, recourse to empirical tuning is normally required and its use is widespread. Information about the system noise contribution is held in matrices $Q$ and $R$ and, in essence, the selection of $Q$ and $R$ determines the accuracy and the performance of the filter, since they mutually determine the action of the EKF gain matrix, $K_{k+1}$, and estimation error covariance matrix, $P_{k+1}$. The $R$, covariance matrix of the measurement noise, can be estimated from the knowledge of the battery terminal voltage. The variance is obtained from the square of the

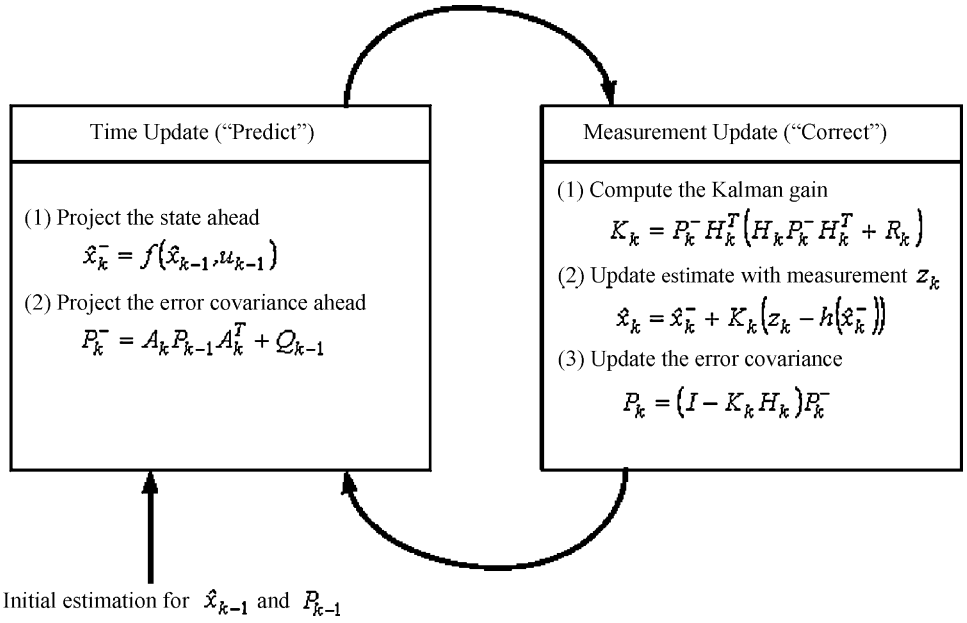


Fig. 7. Recursive EKF algorithm.

root-mean-square (rms) noise at each cell, and is assumed to have Gaussian distribution and be independent.

Initialization of the covariance matrix describing disturbances on the plant ($Q$) is complicated by the fact that knowledge of the model inaccuracies and system disturbances is limited, particularly as each battery has different characteristics. An astute choice of $Q$ is obtained from experimental studies under the simplifying assumption that there is no correlation between the elements of $\sigma_k$ and the noise present on each battery's voltage transducers, thereby leading to a diagonal $Q$. The initial covariance matrix $P_0$ together with $Q$ and $R$, for our case, are ultimately chosen to be

$$P_0 = \begin{bmatrix} 1 & 0 & 0 & 0 \\ 0 & 1 & 0 & 0 \\ 0 & 0 & 1 & 0 \\ 0 & 0 & 0 & 1 \end{bmatrix}, \qquad R = 10,$$

$$Q = \begin{bmatrix} 0.5 & 0 & 0 & 0 \\ 0 & 0.5 & 0 & 0 \\ 0 & 0 & 0.005 & 0 \\ 0 & 0 & 0 & 0.0001 \end{bmatrix} \tag{28}$$

### 3.2. Step 2: parameter identification of the hysteresis model

In order to use the hysteresis model, we need to identify the unknown parameters ($\theta = [\, R^+ \quad E^- \quad M \quad \gamma \,]^{\mathrm{T}}$). Due to nonlinear equations of the hysteresis model, it is necessary to use nonlinear identification methods, such as EKF. To do so, we require a state-space model describing the dynamics of the unknown parameters of the model ($\theta$). We will use the Kalman filter as an optimum observer of these parameter's values, creating an estimate $\hat{\theta}$. In electro-chemical batteries, the actual parameters change very slowly, so we model them as a constant with some small perturbation [7]:

$$\theta_{k+1} = A\theta_k + Bu + r_k \tag{29}$$

where

$$A = \begin{bmatrix} 1 & 0 & 0 & 0 \\ 0 & 1 & 0 & 0 \\ 0 & 0 & 1 & 0 \\ 0 & 0 & 0 & 1 \end{bmatrix}, \qquad B = 0 \tag{30}$$

The small white noise input, $r_k$, is imaginary, but models the slow change in the parameters of the system and the dynamic behavior of the battery. The output equation required for Kalman-filter system identification must be a measurable function of the system parameters. We use

$$d_k = y_k + e_k \tag{31}$$

where $y_k$ is the output equation of the hysteresis model ($y_k = \mathrm{OCV}(\mathrm{SoC}_k) - Ri_k + h_k$), and $e_k$ models both the sensor noise and the modeling error. We compare $y_k$, computed using $\hat{\theta}_k$, with the measured battery output and adapt $\hat{\theta}_k$ to minimize the difference. Now, we can estimate the system parameters by applying EKF to this state-space model and battery data. It is important to notify that the new output equation is still nonlinear in unknown parameters and requires linearization, therefore we introduce $C_k$ as follows:

$$C_k = \left.\frac{\mathrm{d}y_k}{\mathrm{d}\theta}\right|_{\theta=\hat{\theta}_k^-} \tag{32}$$

$\hat{\theta}_k^-$ is a priori estimation of $\theta$ at step $k$.

$$C_k = \frac{\mathrm{d}y(x_k, u_k, \theta)}{\mathrm{d}\theta} = \frac{\partial y(x_k, u_k, \theta)}{\partial \theta} + \frac{\partial y(x_k, u_k, \theta)}{\partial x_k}\frac{\mathrm{d}x_k}{\mathrm{d}\theta}\frac{\mathrm{d}x_k}{\mathrm{d}\theta}$$
$$= \frac{\partial f(x_{k-1}, u_{k-1}, \theta)}{\partial \theta} + \frac{\partial f(x_{k-1}, u_{k-1}, \theta)}{\partial x_{k-1}}\frac{\mathrm{d}x_{k-1}}{\mathrm{d}\theta} \quad (33)$$

For this model we have

$$\frac{\mathrm{d}y(x_k, u_k, \theta)}{\mathrm{d}\theta} = [-i^+ \quad -i^- \quad 0 \quad 0] + \frac{\mathrm{d}h_k}{\mathrm{d}\theta}\frac{\mathrm{d}h_k}{\mathrm{d}\theta}$$
$$= \left[0 \quad 0 \quad (1 - F_{k-1})\,\mathrm{sgn}(i_{k-1}) \quad (M - h_{k-1})\left|\frac{\eta_i i_{k-1}\,\Delta t}{C}\right| F_{k-1}\right] + F_{k-1}\frac{\mathrm{d}h_{k-1}}{\mathrm{d}\theta} \quad (34)$$

where $h_k$, $i^-$, $i^+$, $F$, $\Delta t$, $\eta_i$, $C$ were defined in battery hysteresis model (Section 2.2).To implement this identification method, three sets of data are required:

(1) measurable terminal parameters of the battery ($V_t$, $I_t$),
(2) SoC and OCV which are obtained from the battery RC model, and
(3) hysteresis voltage derived from a static curve.

Now we can simply identify the unknown parameters by applying KF relations (shown in Fig. 7) to our new state-space equations.

### 3.3. Step 3: SoC estimation of the hysteresis model by EKF

After identifying the unknown parameters of the battery hysteresis model, we can easily estimate the model states via EKF. Except for $Q$ and $R$ matrices, this step is similar to Section 3.1. Therefore, in order to avoid redundancy, we neglect the detailed description of this step. As a result the hysteresis voltage is estimated and more accurate values for SoC can be obtained. The relative $Q$ and $R$ matrices are as follows:

$$Q = \begin{bmatrix} 0.01 & 0 \\ 0 & 0.001 \end{bmatrix}, \qquad R = 10 \quad (35)$$

## 4. Simulation results

For experimental tests a 6 V 1 Ah VRLA battery, manufactured by Optima-Palma Co., is used as a case study. These tests have been carried out by a battery test unit Solartron 1470. The maximum current of the test unit is limited to 4 A, so we have to scale the battery current to 1/25 in Toyota Prius where Ni-MH batteries have been replaced with 25 Ah lead-acid batteries [24].

### 4.1. Experimental tests

In this section the capability and the accuracy of the proposed method in estimating SoC is verified by two experimental tests, and finally the obtained results are compared with the Ah counting method and RC modeling technique.

#### 4.1.1. Model validation test

Here, we assess the proposed model validity by a discharge pulse current of 1/5$C$ (A). Our criterion for the model accuracy is the difference between the measured and estimated terminal voltage, the smaller error indicates the better accuracy [2]. The current profile, measured and estimated terminal voltages and their errors are shown in Figs. 8 and 9.

As shown in Fig. 9, it is apparent that the estimated output voltage error is less than 60 mV which shows the model is able to estimate the model states accurately.

#### 4.1.2. The main test

In this test the capability of the proposed model in HEV application is examined. To do so, six successive NYCC driving cycles are applied to Toyota Prius with 25 Ah lead-acid batteries [24] where the initial SoC of the batteries is 0.9. As the case study battery is 1 Ah, the battery current is scaled to 1/25. NYCC driving cycle and its related battery current are shown in Figs. 10 and 11.

The input current of the case study battery (scaled current), measured and estimated terminal voltages are illustrated in Figs. 12 and 13.

The error between the measured and the estimated output voltage is shown in Fig. 13(b). The error is approximately 0.3 V which is acceptable for HEV application due to fast deviation of the battery current.

Fig. 14(a) shows the SoC obtained from the combined model, Ah counting method, and RC modeling technique. The SoC obtained from the combined model shows an estimation error within 2% in comparison with Ah counting, as a reference method (Fig. 14(b)); even better results can be achieved if the initial transience caused by inaccurate initial values is ignored. The estimation error of SoC in RC model compared with Ah counting method is shown in Fig. 14(c). The results indicate that the proposed approach can yield to better SoC results in comparison with those obtained using conventional techniques such as Ah counting and RC modeling (equivalent circuit).

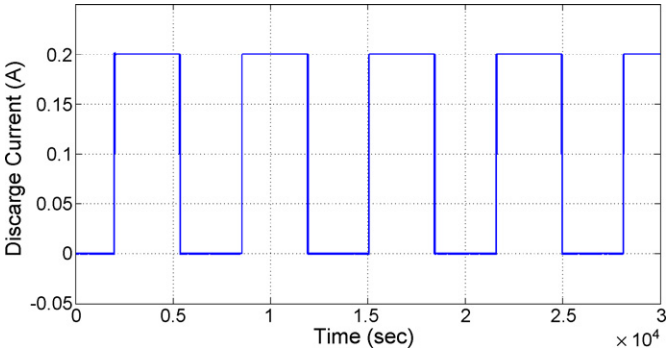


Fig. 8. Battery current profile in validation test.

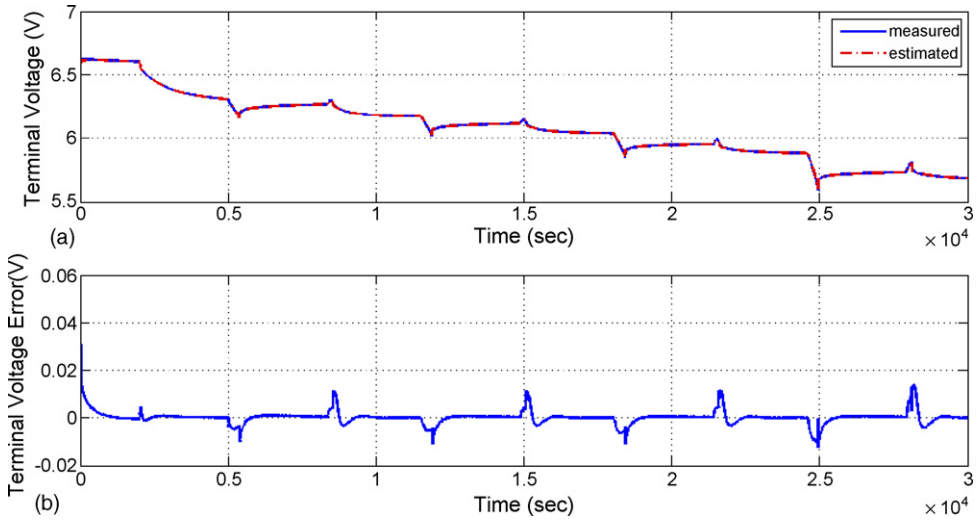


Fig. 9. (a) Measured and estimated battery terminal voltage in validation test. (b) Error between the measured and the estimated battery terminal voltage.

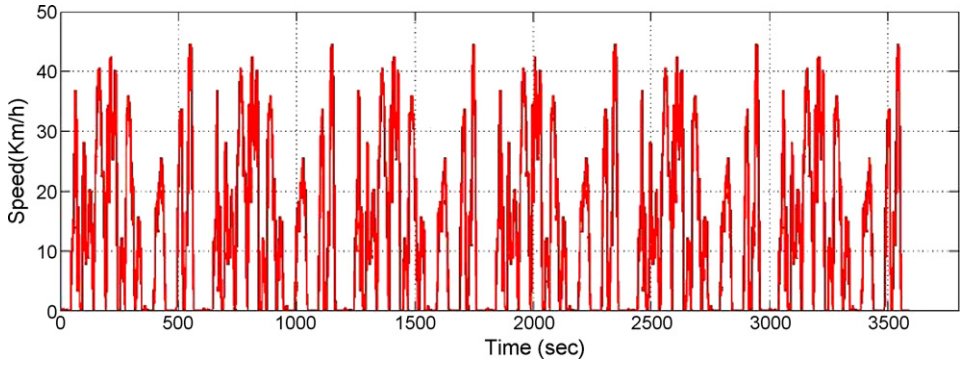


Fig. 10. Six successive NYCC driving cycles [24].

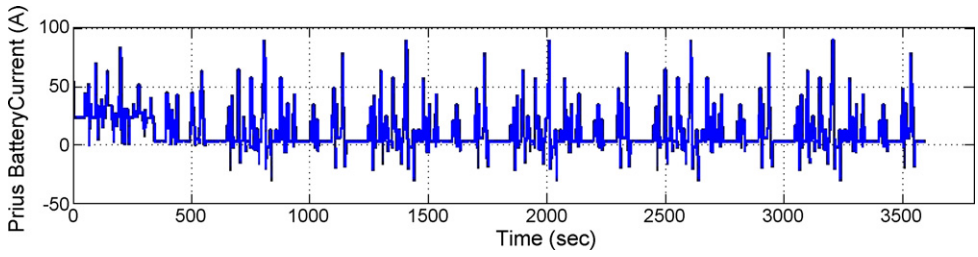


Fig. 11. Battery current in Toyota Prius.

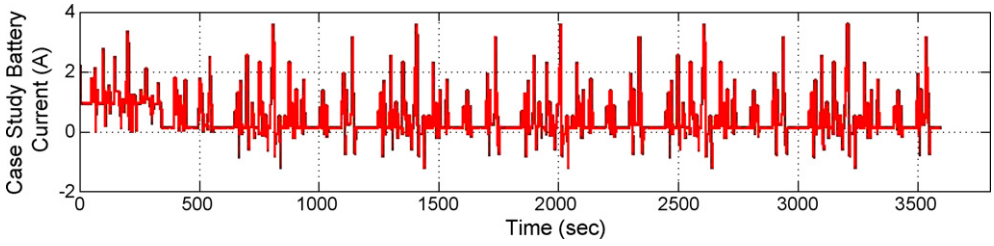


Fig. 12. Battery current case study.

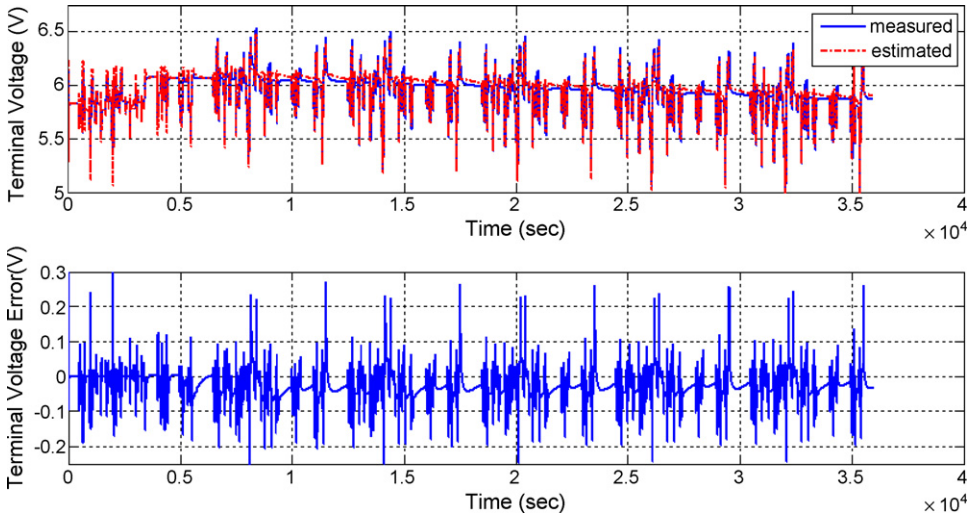


Fig. 13. (a) Measured and estimated battery terminal voltage in the main test. (b) Error between the measured and the estimated battery terminal voltage.

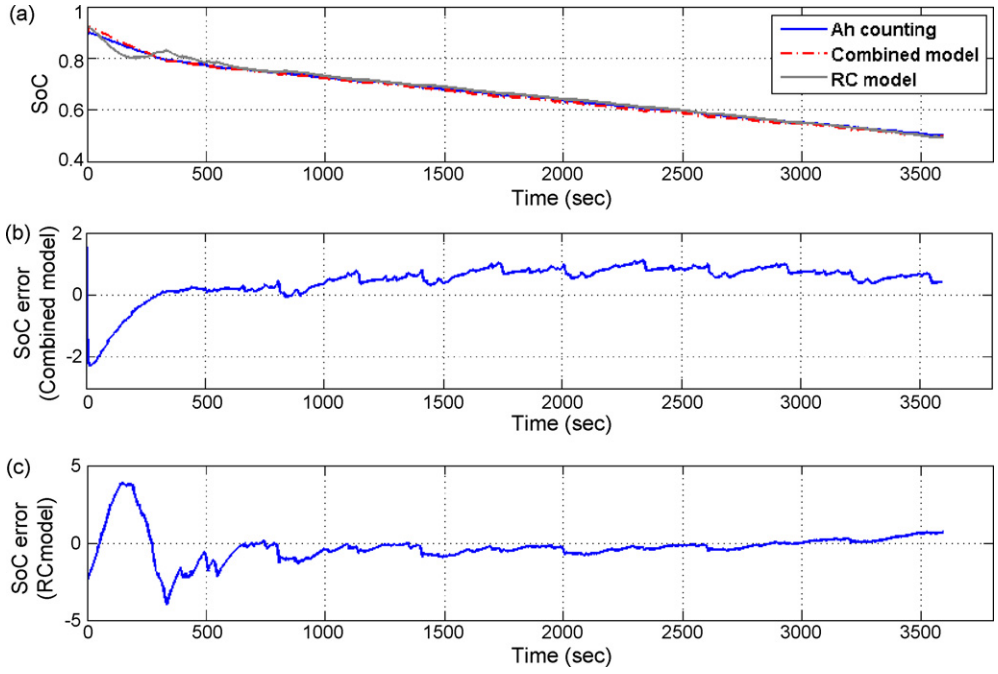


Fig. 14. (a) The SoC obtained from the combined model, Ah counting method, and RC modeling technique. (b) Error between the SoC estimated from the combined model and Ah counting method. (c) Error between the SoC estimated from the RC modeling technique and Ah counting method.

## 5. Conclusion

In this paper a novel combined model for lead-acid batteries has been presented, and then an EKF-based algorithm has been developed to estimate SoC. The proposed method can accurately model the dynamic behavior of the battery which makes it appropriate for HEV application. The capability of the proposed model has been verified by two experimental tests, the validation test with pulse current and the main test which is applied to Toyota Prius in NYCC driving cycle. The presented tests have shown that the proposed method gives SoC estimation with the error less than 2%. The results reveal that the proposed method shows a great performance when it is compared with other conventional methods such as Ah counting and RC modeling (equivalent circuit). However, the proposed method, like other methods, has limitations in low temperatures and very high discharge rates.

## Acknowledgment

The authors gratefully acknowledge M. Fesanghary for his valuable suggestions and discussions.

## References

[1] D. Berndt, Maintenance-Free Batteries, John Wiley, New York, 1993.
[2] B.S. Bhangu, P. Bentley, P. Bentley, D.A. Stone, C.M. Bingham, IEEE Trans. Vehicular Technol. 54 (3) (2005).

[3] O. Caumont, Ph. Le Moigne, P. Lenain, C. Rombaut, Proceedings of Electric Vehicle Symposium, Brussels, Belgium, September–October 1998.
[4] R. Giglioli, P. Pelacchi, M. Raugi, G. Zini, Energia Elettrica 65 (1) (1988) 27–33.
[5] J. Alzieu, H. Smimite, D. Glaize, J. Power Sources 67 (1997) 157–161.
[6] G. Plett, J. Power Sources 134 (2) (2004) 252–261.
[7] G. Plett, J. Power Sources 134 (2) (2004) 262–276.
[8] G. Plett, J. Power Sources 134 (2) (2004) 277–292.
[9] P. Singh, C. Fennie, D.E. Reisner, A. Salkind, Proceedings of Electric Vehicle Symposium, Brussels, Belgium, September–October 1998.
[10] P. Singh, C. Fennie, D. Reisner, A. Salkind, Proceedings of the 15th Annual Battery Conference on Applications and Advances, Long Beach, CA, USA, January 11–14, 2000, pp. 199–204.
[11] F. Huet, J. Power Sources 70 (1998) 59–69.
[12] S. Rodrigues, N. Munichandraiah, A.K. Shukla, J. Power Sources 87 (2000) 12–20.
[13] C. Cai, D. Du, Z. Liu, J. Ge, Proceedings of the 9th International Conference on Neural Information Processing (ICONIP'2002), vol. 2, 2002.
[14] C.C. Chan, E.W.C. Lo, S. Weixiang, J. Power Sources 87 (2000) 201–204.
[15] P. Singh, C. Fennie Jr., D. Reisner, J. Power Sources 136 (2004) 322–333.
[16] S. Arey, V.R. Gaddam, Z. Yang, P. Singh, C. Fennie Jr., D.E. Reisner, Proceedings of the EVS-16, Beijing, PR China, October 14–16, 1999.
[17] G.O. Patillon, J.N. d'Alché-Buc, Artificial Neural Networks ICANN'97 7th International Conference, vol. 1327, Berlin, Germany, 1997, pp. 1095–1100.
[18] O. Barbarisi, F. Vasca, L. Glielmo, J. Control Eng. Pract. 14 (2006) 267–275.
[19] C.Y. Tseng, Ch.F. Lin, J. Power Sources 147 (2005) 282–287.
[20] J. Chiasson, B. Vairamohan, IEEE Trans. Control Syst. Technol. 13 (3) (2005).
[21] S. Piller, M. Perrin, A. Jossen, J. Power Sources 96 (2001) 113–120.
[22] K. Takano, K. Nozaki, Y. Saito, A. Negishi, K. Kato, Y. Yamaguchi, J. Power Sources 90 (2) (2000) 214–223.
[23] V. Pop, H.J. Bergveld, P.H.L. Notten, P.P.L. Regtien, Meas. Sci. Technol. 16 (2005) R93–R110.
[24] S.R. Bhatikar, R.L. Mahajan, K. Wipke, V. Johnson, Advance Vehicle Simulator (Advisor), Nat. Renewable Energy Lab., Golden, CO, 2002. Online: www.ctts.nrel.gov/advisor.
[25] M.S. Grewal, Kalman Filtering: Theory and Practice Using Matlab, 2nd ed., John Wiley & Sons, New York, 2001, pp. 114–200.
[26] S. Haykin, Adaptive Filter Theory, 3rd ed., Prentice Hall, 2000, pp. 302–334.
[27] V. Srinivasan, J. Weidner, J. Newman, J. Electrochem. Soc. 148 (9) (2001) A969–A980.